Supporting Information

Superhydrophobic and mechanical properties enhanced the electrospinning film with a multiscale micro-nano structure for high-efficiency radiation cooling

Lijing Kong [a,b], Puqing Sun [a,b], Jincheng Liu [a,b], Yongxing Lin [b], Chao Xiao [b], Chao bao [b], Kang Zheng [b], Meng Xue [c], Xian Zhang [b], Xianglan Liu [b,*], Xingyou Tian [b,*]

[a] Institutes of Physical Science and Information Technology, Anhui University, Hefei, 230601, PR China
[b] Key Lab of Photovoltaic and Energy Conservation Materials, Institute of Solid State Physics, HFIPS, Chinese Academy of Sciences, Hefei, 230031, China
[c] Guangdong Banggu Film Coatings Innovation Academy Co., Ltd., Nanxiong 512400, China

*Corresponding author.
E-mail addresses: xlliu@issp.ac.cn (X. Liu), xytian@issp.ac.cn (X. Tian).

1. EXPERIMENTAL SECTION

1.1. Materials and Method

Acetone (AR, ≥ 99.5%) was purchased from Shanghai Sinopharm Chemical Reagent Co., LTD. Nanometer zirconia (≤ 100 nm), nanometer titanium dioxide (≤100 nm, rutile type), nanometer zinc oxide (50 ± 10 nm), Tetrahydrofuran (THF, ≥99.5%), Nile Blue A, and N, N dimethylformamide (DMF, AR, 99.5%) were purchased from Aladdin Biochemical Technology Co., LTD. Nano silica (50 nm) was purchased from Xuan Cheng Jing Rui New Materials Co., LTD., China. Polyvinylidene fluoride (PVDF, MW = 400000) and nano-aluminum oxide (α about 95%, γ about 5%, 80 nm) were purchased from Shanghai Maclin Biochemical Co., LTD., China. Orange silicone was purchased from Suzhou Wuzhong District Sheng da desiccant factory. Sylgard184 prepolymer (PDMS) from Dow Corning Silicone Co., LTD.; the weight ratio of prepolymer to curing agent is 10∶1.

The preparation for the ZrPF film is as follows: Firstly, PVDF film was prepared by electrospinning. PVDF powders were added in a mixed solvent of DMF and acetone. The volume ratio of DMF and acetone is 5:3. Then the mixture was stirred at 70 °C for 12 h to obtain a homogeneous solution as the electrospinning dope. In the electrospinning process, the distance between the needle and the accepting board was adjusted to 18 cm, the spinning voltage was 16 kV, and the injection speed was 4000 μl/h. The ambient temperature was 25 - 30 °C and the humidity was 50 - 60%. After electrospinning, the prepared film was placed in an oven at 60 °C for 2 h. The obtained sample was labeled as F-S. For comparison, the dense film was prepared by pouring the spinning dope into a 60 mm × 60 mm × 1 mm glass mold. After the natural

volatilization of the solvent, the PVDF film formed and was labeled as F-W.

Sequentially, the PVDF electrospinning film was laminated. The F-S film was curled and folded in one direction, then cold pressed for 3 s under a pressure of 0.1 MPa. This sample was labeled as PF-S. The thicknesses and sizes were adjusted by changing the spinning times and folding times.

Finally, the ZrPF film was prepared. PDMS and nano-zirconia particles were dispersed in THF to prepare solution A and solution B, respectively. Then solution A and B were mixed and ultrasonicated for 1 hour. Nextly, the prepared PF-S film was soaked in AB mixed solution for 20 min. After that, the as-prepared ZrPF film was washed by ethanol and dried at 80 ℃ for 3 h. The contribution of PDMS was also investigated by altering the PDMS contents to 0.5, 1, 1.5, 2, 2.5, 3, 3.5, and 4 wt%, the corresponding solution were labeled as 0.5 A, 1 A, 1.5 A, 2 A, 2.5 A, 3 A, 3.5 A, and 4 A, respectively. Meanwhile, the contribution of ZrO_2 was also investigated by altering the ZrO_2 contents to 0.5, 1, 1.5, 2, 2.5, and 3 wt%, and the corresponding solution were labeled as 0.5 B, 1 B, 1.5 B, 2 B, 2.5 B, and 3 B, respectively.

Additionally, in order to verify that this method is also suitable for other particles to prepare the multi-scale micro-nano structure film for excellent radiation refrigeration. The above preparation process was repeated with alumina, titanium oxide, zinc oxide, and silicon oxide, and the corresponding product was labeled as AlPF, TiPF, ZnPF, and SiPF, respectively.

1.2. Characterization of the ZrPF Film

The SEM test sample is securely affixed to the SEM test bench using conductive

tape. Subsequently, the ion sputtering gold spray instrument (k550x, Nanjing Qinsi Technology Co., LTD) is employed to sputter with a current of 30 mA for a duration of 3 min. The morphology and element distribution of ZrPF films were characterized by a field-emission scanning electron microscope (SU8020, Hitachi High Technologies Corporation) equipped with an energy-dispersive X-ray spectroscope. The SEM image is acquired using a voltage of 10 kV. The ZrPF film element distribution is obtained by collecting element signals continuously for 3min with a voltage of 15 kV.

The sizes of the F-S fiber, ZrO_2 particles, and ZrPF fiber were measured using the software Nano Measurer 1.2. The solar (0.3 - 2.5 μm) reflectance spectra of samples were characterized by a UV−VIS−NIR spectrometer (Lambda 1050+, Perkin Elmer) equipped with polytetrafluoroethylene (PTFE) integrating sphere, and the thermal (2.5 - 15 μm) emittance spectra were measured using a Fourier transform infrared spectrometer (Nicolet iS50, Thermo Fisher Scientific) with a diffuse gold integrating sphere. Fourier transform infrared (FT-IR) spectrometer (Spectrum Two, Perkin Elmer) was used to determine the functional groups of ZrPF films in the atmospheric windows. The refractive index and extinction coefficient of samples were measured by ellipsometer (HORIBA France SAS). Thermal conductivity of the ZrPF film was calculated by the following equation $K = \alpha \cdot C_p \cdot \rho$, where C_p is the specific heat (J/g·K), ρ is the density(g/cm^3), and α is the thermal diffusivity(m^2/s). The α of ZrPF films was measured by laser thermal conductivity meter (LFA467/HFM446S, NETZSCH) at room temperature 25 ℃. The number of flashes was set to 5. Each sample was measured three times and averaged. C_p was measured using thermal differential scanning

calorimeter (DSC, Q2000, TA, America).

1.3. Radiation Cooling Performance Test Indoor

The indoor simulated solar light source intensity of 1000 W/m^2, employing an Air Mass 1.5 Global (AM 1.5 G) solar simulator (94043A), and the infrared thermal imager (227s, FOTRIC) was used to record real-time thermal imaging and track temperature changes. In addition, there is a silicone rubber heating pad with 100 W/m^2 power to simulate the metabolic heat production of the skin.

1.4. Radiation Cooling Performance Test Outdoor

Outdoor experiments were carried out to evaluate and investigate the radiative cooling performance of ZrPF films in Hefei, Anhui (31°51'23.816"N, 117°8'9.743"E), China, from August 18 to 26, 2023. A self-designed test device was placed in an open space on the roof and the device was about 25 cm away from the ground to reduce the influence of hot air convection caused by the extremely heated ground.

A multichannel temperature data logger (TA612C, Suzhou Tans electronic Industrial Co., LTD) was also used to record the temperature changes. Solar irradiance measurements were recorded using a solar irradiance meter (TES-1333R, Taishi Electronic Industry Co., LTD). Temperature data and irradiance data are obtained every 30 seconds. The outdoor experiments were conducted

In total, there were two groups of control experiments. one group, a ZrPF film (3 cm × 3 cm) was laid on the hollow foam, and the surface of the ZrPF film was covered with a layer of transparent polyethylene (PE) film. The thermocouple and 100 W/m^2 silicone rubber heating gasket are placed successively under the foam block. The

silicone rubber heating gaskets are used to heat production of simulate skin metabolism. In a similar setting, when the ZrPF film is not placed, the measured temperature is used as the simulated bare skin temperature. In the other group, the silicone rubber heating gasket was omitted while keeping all other settings constant. When the ZrPF film was not applied, the measured temperature served as the ambient temperature.

1.5. Calculation of the Cooling Power

The net cooling power of the ZrPF film was calculated using MATLAB and the following thermal equilibrium equation consisting of four power terms:

$$P_{cooling} = P_{rad} - P_{atm} - P_{solar} - P_{non-rad} \quad (1)$$

where P_{rad}, P_{atm}, P_{solar}, and $P_{non-rad}$ are the thermal radiation energies released from the sample, the thermal radiation energy transmitted from the atmosphere to the sample, the solar radiation energy absorbed by the sample, and the non-radiative heat transfer from the sample to the atmosphere via conduction and convection, respectively. Specifically, the thermal radiation power P_{rad} can be defined by the following equation:

$$P_{rad} = \int d\Omega \, cos\theta d\theta \int_0^{\infty} d\lambda I_{BB}(\lambda, T_{rad}) \, \varepsilon(\lambda, \theta) \quad (2)$$

where $\int d\Omega = 2\pi \int_0^{2\pi} d\varphi \int_0^{\frac{\pi}{2}} sin\theta d\theta = 2\pi \int_0^{\frac{\pi}{2}} sin\theta d\theta$, is the angular integral over a hemisphere, and $\varepsilon(\lambda, \theta)$ indicates the spectral and angular emissivity of the sample.

The spectral emittance of a blackbody at absolute temperature T is given by Planck's formula:

$$I_{BB}(\lambda, T_{rad}) = (2hc^2/\lambda^5)/[e^{(hc/\lambda \kappa_B T_{rad})} - 1] \quad (3)$$

and h is Planck's constant, c is the speed of light in vacuum, κ_B is the Boltzmann constant, and λ is the wavelength.

Furthermore, the power absorbed by the atmosphere (P_{atm}) at the ambient temperature (T_{amb}) is given by the following equation:

$$P_{atm} = \int d\Omega \, cos\theta d\theta \int_0^\infty d\lambda I_{BB}(\lambda, T_{amb}) \, \varepsilon(\lambda, \theta) \varepsilon_{atm}(\lambda, \theta) \tag{4}$$

where $I_{BB}(\lambda, T_{amb})$ denotes the spectral radiance of a blackbody at atmospheric temperature:

$$I_{BB}(\lambda, T_{atm}) = (2hc^2/\lambda^5)/[e^{(hc/\lambda \kappa_B T_{atm})} - 1] \tag{5}$$

and the atmospheric emissivity is given by

$$\varepsilon_{atm}(\lambda, \theta) = 1 - t(\lambda)^{1/cos\theta} \tag{6}$$

Additionally, the solar power (P_{solar}) absorbed by a radiative cooler is given by

$$P_{solar} = \int_0^\infty d\lambda \, \varepsilon(\lambda, \theta) I_{AM1.5}(\lambda) \tag{7}$$

Here, $t(\lambda)^{1/cos\theta}$ is the atmospheric transmittance at the zenith angle at Mauna Kea [1, 2]. $\varepsilon(\lambda, \theta) = 1 - \bar{R}_{\text{solar}}$ is the surface's spectral thermal emittance at wavelength λ, we assume the ZrPF film is facing the sun, $\theta = 0$. Thus, the term P_{solar} does not have an angular integral [3, 4], and the terrestrial solar irradiance on the surface is represented by the AM1.5G (Air Mass 1.5 Global) spectra.

The final Eq. (7) simplifies to $P_{solar} = (1 - \bar{R}_{\text{solar}}) I_{AM1.5}$ [1, 5, 6].

Finally,

$$P_{non-rad} = q(T_{amb} - T_{rad}) \tag{8}$$

where $q = q_{cond} + q_{conv}$ is the heat transfer coefficient, and the nonradiative power ($P_{non-rad}$) is determined by heat transfer between the ZrPF film surface and ambient environment. The theoretical cooling power was calculated, assuming a steady ambient environment, the solar irradiance of 1000 W/m^2, and several previous reports

have shown that radiative cooling can effectively inhibit non-radiative heat gain, with an estimated q value range of 3 - 12 $W/m^2 \cdot K$ [4, 7, 8].

1.6. Superhydrophobicity Test

The static water contact angle was measured by using a contact angle measuring instrument (CD-100D, Shanghai All Precision Instrument Co., LTD.) to characterize the surface hydrophobicity of samples with 2 uL water droplets. Sliding angles were tested via homemade tools: place the sample on an inclined plate Nile Blue A solutions was dropped to the surface of samples to investigate the droplets sliding phenomenon.

In the study of slip angle of ZrPF film, we established an experimental setup to measure the sliding angle of the ZrPF film, as demonstrated in the accompanying **Video. 2.** By adjusting the gasket thickness beneath the metal plate, we controlled the tilt angle of the metal plate while using a standard protractor as a reference plate to accurately record its tilt angle. The ZrPF film was placed on the metal plate and liquid droplets were applied onto it. We recorded the tilt angle at which the rapid sliding of liquid droplets occurred on the ZrPF film. This tilt angle is defined as the slip angle.

1.7. Mechanical Property Test

The mechanical tensile properties of F-S, PF-S and ZrPF were tested by electronic universal testing machine (TY-5000) at the speed of 20 mm/min, and each sample was measured 3 times.

1.8. Air Permeability Test

The beaker was filled with orange silica gel (it will turn green when contacted with water). Sealed the beaker mouth with ZrPF film and then placed it in the salt spray

tester (TY/YW-90) for 2 h. Subsequently, observed the color change of the orange silica gel and determined the air permeability of ZrPF.

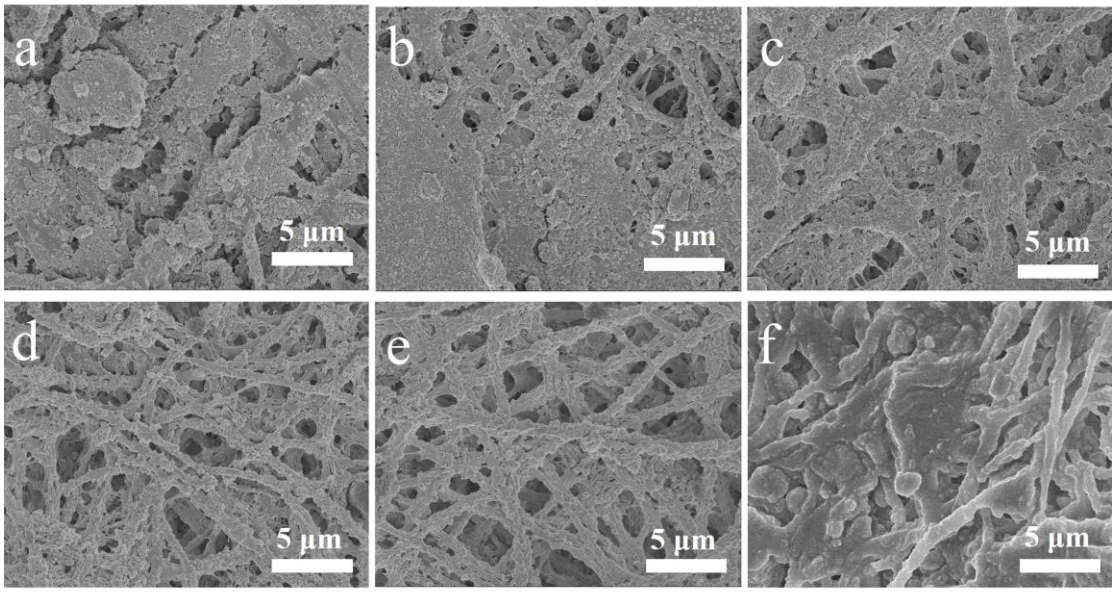

Fig. S1. Effect of PDMS concentration on the morphology of ZrPF. (a-f) The SEM images of ZrPF films prepared from PDMS concentration of 1%, 1.5%, 2%, 2.5%, 3%, and 3.5%, respectively. The ZrO_2 concentration is 1%.

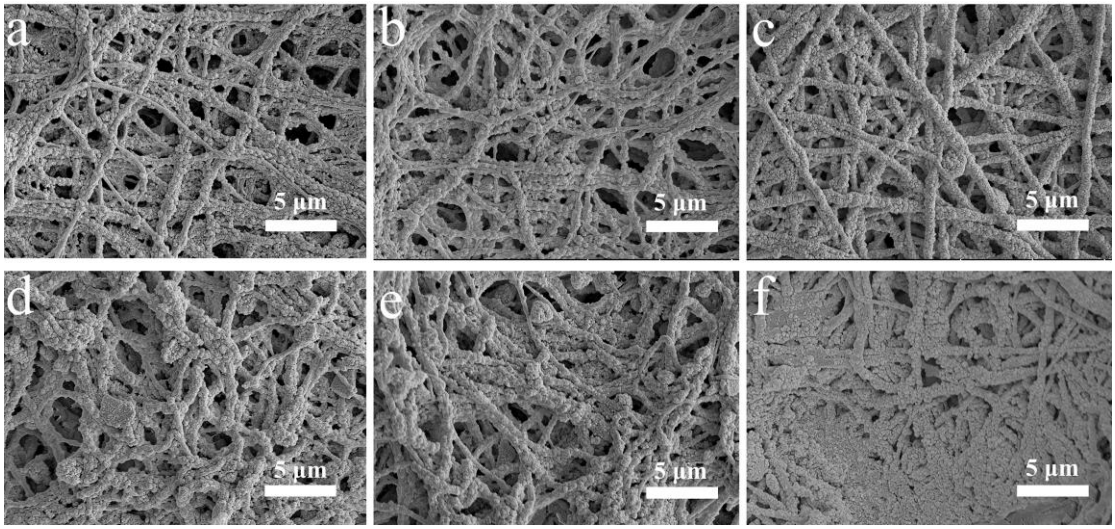

Fig. S2. Effect of ZrO_2 concentration on the morphology of ZrPF. (a-f) The SEM images of ZrPF films fabricated with the ZrO_2 concentration of 0.5%, 1%, 1.5%, 2%, 2.5%, and 3%, respectively. The PDMS concentration is 3%.

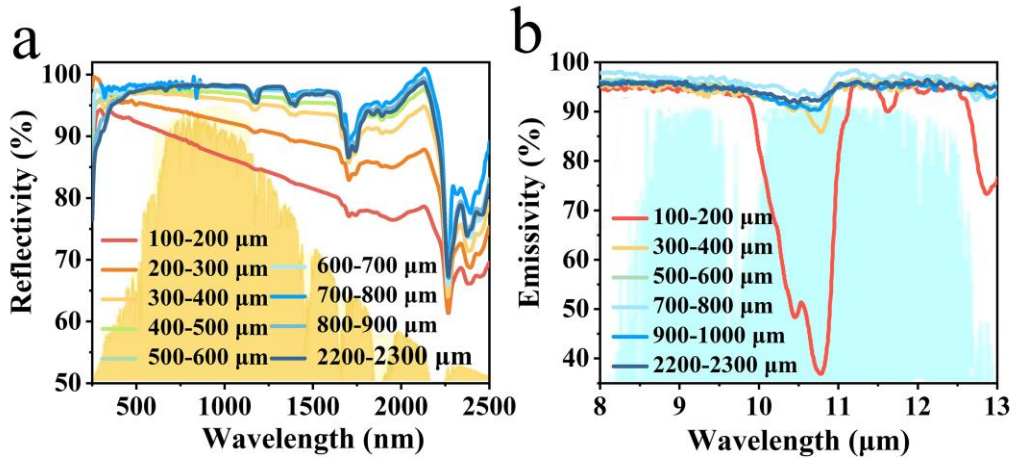

Fig. S3. Effects of the thickness of ZrPF film on the corresponding spectral response of ZrPF film. (a) The reflectance spectra of the ZrPF films as the function of the film thickness. (b) The emissivity spectra as the function of the film thickness. All the samples were prepared with the PDMS concentration of 3 wt% and ZrO_2 concentration of 1.5 wt%.

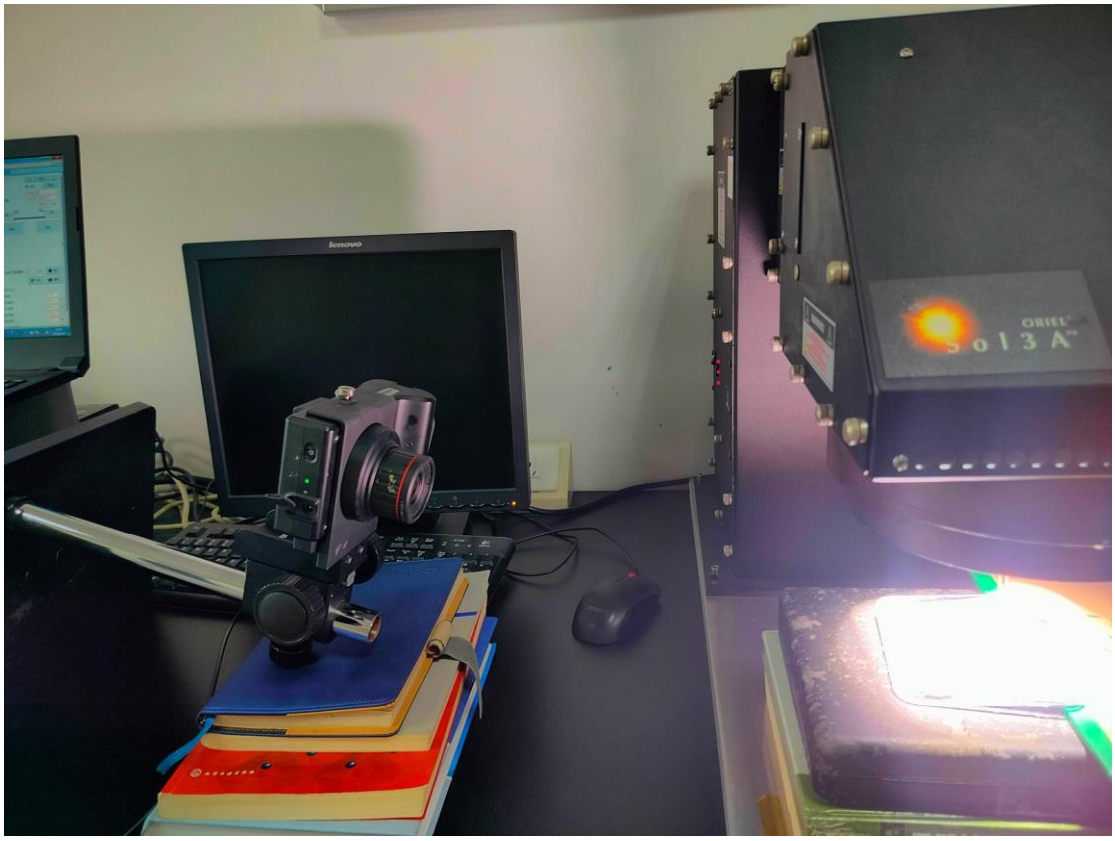

Fig. S4. The photograph of the set-up for the simulated solar radiation refrigeration performance test indoor.

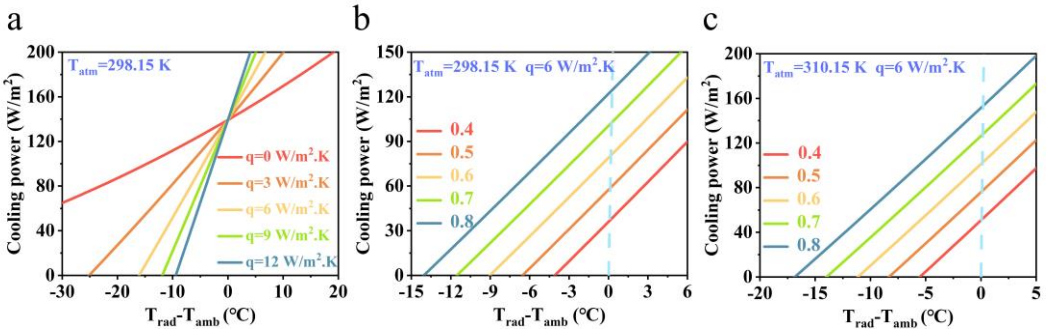

Fig. S5. MATLAB calculation of radiant cooling power. (a) The radiant refrigeration power of ZrPF film under different non-radiative heat transfer coefficients (q) of 0, 3, 6, 9, and 12 $W/m^2 \cdot K$, respectively. The ambient temperature is 298.15 K. (b) The radiant refrigeration power of ZrPF film under different atmospheric transmittance of 0.4, 0.5, 0.6, 0.7, 0.8, respectively. The ambient temperature is 298.15 K, and the non-radiative heat transfer coefficient q is 6 $W/m^2 \cdot K$. (c) The radiant refrigeration power of ZrPF film under different atmospheric transmittance of 0.4, 0.5, 0.6, 0.7, 0.8, respectively. The ambient temperature is 310.15 K, and the non-radiative heat transfer coefficient q is 6 $W/m^2 \cdot K$.

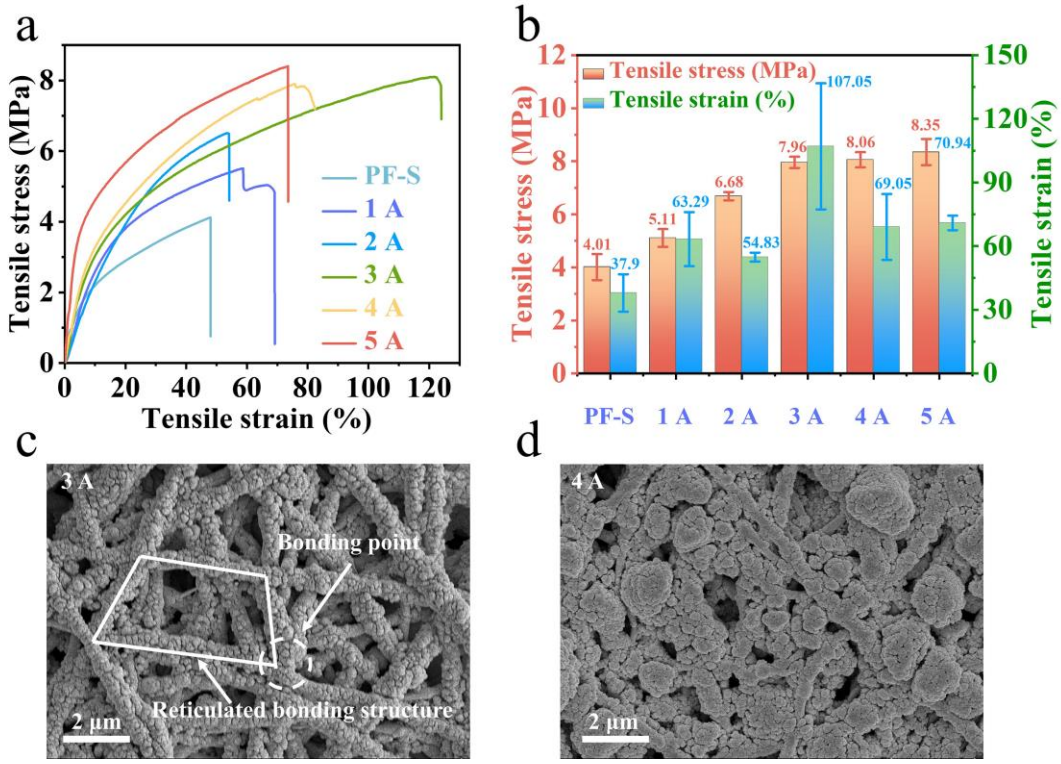

Fig. S6. (a, b) The stress-strain curves and graphs of ZrPF films with different concentrations of PDMS, respectively. The concentration of ZrO_2 is 1.5%. (c, d) SEM images of ZrPF film with PDMS concentration of 3% and 4%, respectively.

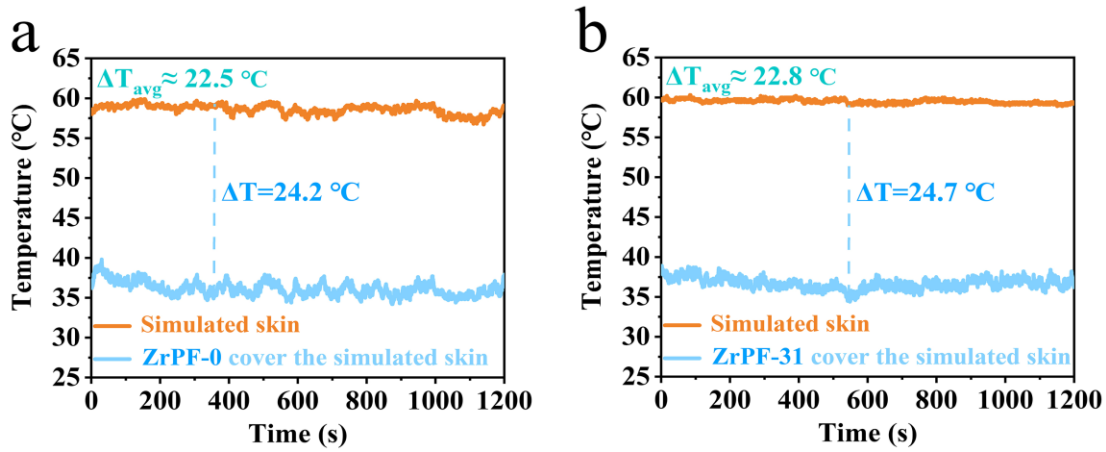

Fig. S7. (a, b) The cooling performance of ZrPF film compared to simulated skin was tested before and after the cycle test, respectively.

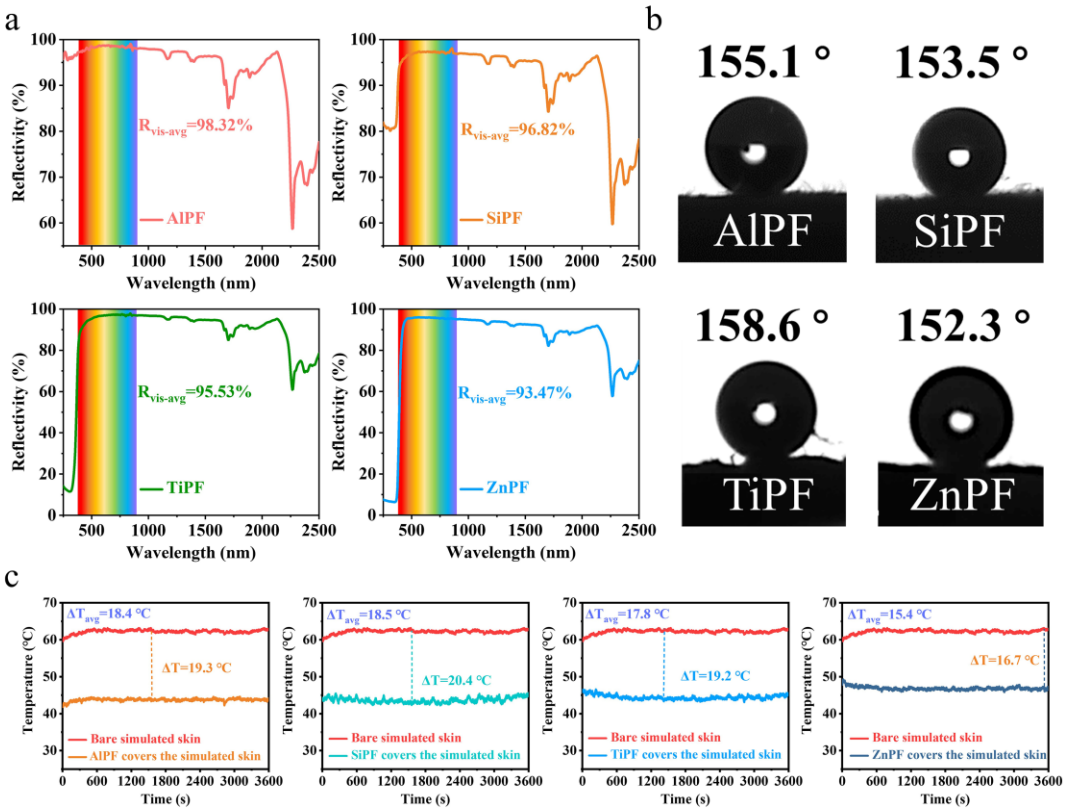

Fig. S8. (a) Solar spectral property of AlPF, SiPF, TiPF, and ZnPF films. (b) Contact angles of AlPF, SiPF, TiPF, and ZnPF films. (c) Outdoor radiation refrigeration performance of AlPF, SiPF, TiPF and ZnPF films for personal cooling.

Tab. S1. The performance comparison of this work with the related researches in recent five years, the red font is the performance of this work.

Material	R/E/T (%)	Test time	I_{Solar} (W/m^2)	Temperature drop (℃)	Mechanical tensile property	CA
PA6/SiO_2 [9]	-/-/85	14:20 - 15:20		Ambient: ΔT_{avg} ~ 1.0 - 2.5 ℃		
PE/PVDF/Si_3N_4 [10]	93.28/ 87.31/-	8h		Simulated skin: Linen: ΔT_{avg} ~ 7.7 ℃, Cotton: ΔT_{avg} ~ 10.4 ℃	Strength: 60 MPa Strain: ~ 40%	116.9 °
PAN [11]	95/-/70	11:00 - 16:00	960	Black body: ΔT ~ 50.8 ℃		
PVDF/Al_2O_3 [12]	97/95/-	11:00 - 12:00	Average solar irradiance 850	Ambient: ΔT_{avg} ~ 4 ℃	Strength: 1.5 MPa Strain: ~80%	144.1 ± 0.6 °
Silk/Al_2O_3 [13]	95/90/-	11:00- 15:00	800 >900	Ambient: ΔT_{avg} ~ 5 ℃, Simulated skin: ΔT_{avg} ~ 19 ℃ Ambient: ΔT_{avg} ~ 3.5 ℃ Simulated skin: ΔT_{avg} ~ 8 ℃		
PU/Si_3N_4 [14]	91/93/-	12:00	1034	Simulated skin: ΔT_{max} ~ 15.9℃ Cotton: ΔT_{max} ~ 21.9 ℃	Strength: 2 MPa Strain: ~ 50% Cycle 1000 times	135 °
PE/ZnO [15]	91/-/81	11:45 - 14:00	750	Simulated skin: ΔT_{avg} ~ 11 ℃, Cotton: ΔT_{avg} ~ 9 ℃	Strength: 6.1 MPa	
PVDF/TiO_2 [16]	93.02/ 89.91/-	12:14	787	Day, Ambient: ΔT_{max} ~ 6.9 ℃ Night, Ambient: ΔT_{max} ~ 4.4 ℃		143.8 °
SF [17]	95/95/-	April 10, 22:00- April 12, 6:00	778	Day, Ambient: ΔT~ 3.8℃ Night, Ambient: ΔT~ 6.4℃	Strength: < 6 MPa Strain: < 5%	
PVDF-HFP [18]	93.7/ 91.9/-	12:00	950	Simulated skin: ΔT ~ 19.8 ℃ Cotton fabric: ΔT ~ 13.2 ℃	Strength: < 1.2 MPa Strain < 30%	
PVDF/PDMS/ZrO_2	95/96/-	13:00- 15:00	1012	Simulated skin: ΔT_{avg} ~ 21.8 ℃ ΔT_{max} ~ 28.5 ℃ Ambient: ΔT_{avg} ~ 7.1 ℃ ΔT_{max} ~ 10.4 ℃	Strength: 8.1 MPa Strain: 124%	>155 °

Video. 1. A boat folded from ZrPF film.

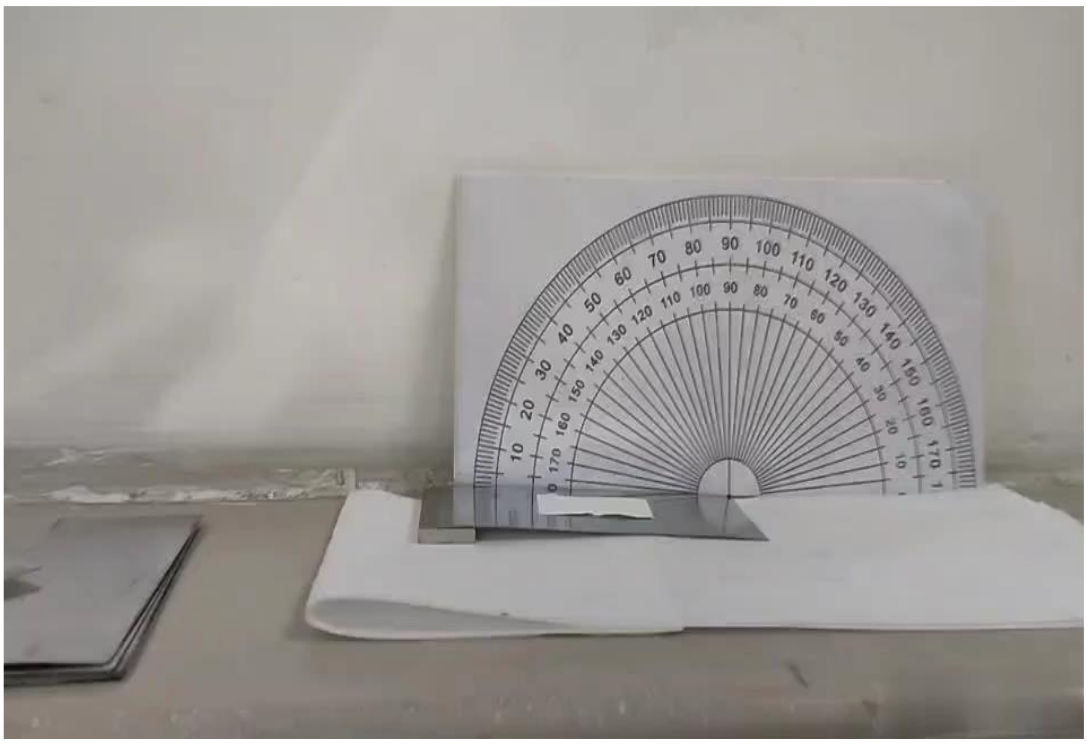

Video. 2. Measurement of the sliding angle on the ZrPF film surface, and the rolling process of water drops on the ZrPF film surface was recorded.

References

1. J.-W. Cho, E.-J. Lee and S.-K. Kim, *Nano Letters*, 2021, **22**, 380-388.
2. Gemini Observatory. IR transmission spectra;, https://www.gemini.edu/observing/telescopes-and-sites/sites#Transmission, (accessed 2023-9-18, 2023).
3. X. Wang, X. Liu, Z. Li, H. Zhang, Z. Yang, H. Zhou and T. Fan, *Advanced Functional Materials*, 2019, **30,** 1907562.
4. C. Cai, Z. Wei, C. Ding, B. Sun, W. Chen, C. Gerhard, E. Nimerovsky, Y. Fu and K. Zhang, *Nano Letters*, 2022, **22**, 4106-4114.
5. Z. Yang, Y. Jia and J. Zhang, *ACS Applied Materials & Interfaces*, 2022, **14**, 24755-24765.
6. J. Mandal, Y. Fu, A. C. Overvig, M. Jia, K. Sun, N. N. Shi, H. Zhou, X. Xiao, N. Yu and Y. Yang, *Science*, 2018, **362**, 315-319.
7. C. Park, C. Park, X. Nie, J. Lee, Y. S. Kim and Y. Yoo, *ACS Sustainable Chemistry & Engineering*, 2022, **10**, 7091-7099.
8. T. Wang, Y. Wu, L. Shi, X. Hu, M. Chen and L. Wu, *Nature Communications*, 2021, **12,** 365.
9. Y. Lu, X. Xiao, J. Fu, C. Huan, S. Qi, Y. Zhan, Y. Zhu and G. Xu, *Chemical Engineering Journal*, 2019, **355**, 532-539.
10. Y.-N. Song, M.-Q. Lei, L.-F. Deng, J. Lei and Z.-M. Li, *ACS Applied Polymer Materials*, 2020, **2**, 4379-4386.
11. H. Kim, S. McSherry, B. Brown and A. Lenert, *ACS Applied Materials & Interfaces*, 2020, **12**, 43553-43559.
12. W. Jing, S. Zhang, W. Zhang, Z. Chen, C. Zhang, D. Wu, Y. Gao and H. Zhu, *ACS Applied Materials & Interfaces*, 2021, **13**, 29558-29566.
13. B. Zhu, W. Li, Q. Zhang, D. Li, X. Liu, Y. Wang, N. Xu, Z. Wu, J. Li, X. Li, P. B. Catrysse, W. Xu, S. Fan and J. Zhu, *Nature Nanotechnology*, 2021, **16**, 1342-1348.
14. D. Miao, N. Cheng, X. Wang, J. Yu and B. Ding, *Nano Letters*, 2022, **22**, 680-687.
15. M. I. Iqbal, K. Lin, F. Sun, S. Chen, A. Pan, H. H. Lee, C.-W. Kan, C. S. K. Lin and C. Y. Tso, *ACS Applied Materials & Interfaces*, 2022, **14**, 23577-23587.
16. N. Li, L. Wei, M. You, M. Chen, H. Li, H. Liu, Z. Fang and H. Bao, *Solar Energy*, 2023, **259**, 41-48.
17. J. He, Q. Zhang, Y. Wu, Y. Ju, Y. Wang and S. Tang, *Chemical Engineering Journal*, 2023, **466**, 143127.
18. N. Cheng, D. Miao, C. Wang, Y. Lin, A. A. Babar, X. Wang, Z. Wang, J. Yu and B. Ding, *Chemical Engineering Journal*, 2023, **460,** 141581.